Published in final edited form as:

Science. 2022 February 25; 375(6583): 859–863. doi:10.1126/science.aaz8777.

Trained ILC3 responses promote intestinal defense

Nicolas Serafini[1], **Angélique Jarade**[1], **Laura Surace**[1], **Pedro Goncalves**[1], **Odile Sismeiro**[2], **Hugo Varet**[2,3], **Rachel Legendre**[2,3], **Jean-Yves Coppee**[2], **Olivier Disson**[4], **Scott K. Durum**[5], **Gad Frankel**[6], **James P. Di Santo**[1,*]

[1]Institut Pasteur, Université de Paris, Inserm U1223, Innate Immunity Unit, Paris, France.

[2]Institut Pasteur, Université de Paris, Transcriptome and Epigenome Platform–Biomics Pole, Paris, France.

[3]Institut Pasteur, Université de Paris, Bioinformatics and Biostatistics Hub, Paris, France.

[4]Institut Pasteur, Université de Paris, Inserm U1117, Biology of Infection Unit, Paris, France.

[5]Laboratory of Cancer and Immunometabolism, Center for Cancer Research, National Cancer Institute, National Institutes of Health, Frederick, MD, USA.

[6]MRC Centre for Molecular Bacteriology and Infection, Department of Life Sciences, Imperial College London, London, UK.

Abstract

Group 3 innate lymphoid cells (ILC3s) are innate immune effectors that contribute to host defense. Whether ILC3 functions are stably modified after pathogen encounter is unknown. Here, we assess the impact of a time-restricted enterobacterial challenge to long-term ILC3 activation in mice. We found that intestinal ILC3s persist for months in an activated state after exposure to *Citrobacter rodentium*. Upon rechallenge, these “trained” ILC3s proliferate, display enhanced interleukin-22 (IL-22) responses, and have a superior capacity to control infection compared with naïve ILC3s. Metabolic changes occur in *C. rodentium*–exposed ILC3s, but only trained ILC3s have an enhanced proliferative capacity that contributes to increased IL-22 production. Accordingly, a limited encounter with a pathogen can promote durable phenotypic and functional changes in intestinal ILC3s that contribute to long-term mucosal defense.

Specialized immune cells promote barrier function and maintain microbial tolerance at mucosal surfaces (1); these include effector and memory T cells that provide long-term immune-surveillance and recall responses as well as diverse innate lymphoid cells (ILCs) (2, 3). Group 3 ILCs (ILC3s) are highly enriched in the gut where they orchestrate lymphoid tissue development and mucosal defense (3, 4). Largely devoid of pattern recognition receptors (5), ILC3s are indirectly activated after infection by soluble factors [interleukin-1β (IL-1β) and IL-23] derived from epithelial and hematopoietic sentinel cells (4) and, in turn,

[*]**Corresponding author:** james.di-santo@pasteur.fr.

Author contributions: N.S. and J.P.D. designed the study and wrote the manuscript. N.S. and A.J. designed, performed, and analyzed the experiments. O.D. assisted with the *Listeria* experiments. P.G. analyzed the microbiota. N.S., O.S., H.V., R.L., and J.-Y.C. performed RNA-seq analysis. L.S. provided metabolism expertise. G.F. provided microbiology expertise. J.P.D. directed the study.

Competing interests: The authors declare no competing financial interests.

secrete IL-17 and IL-22 to protect the host (6–9). ILC3s are active during fetal lymphoid tissue organogenesis (10, 11), and initial encounters with microbial flora in early postnatal life modifies ILC3 subset distribution and cytokine production (6, 12). Whether ILC3s exhibit any degree of long-term adaptation to a commensal or pathogen encounter that results in heightened immunological function remains to be demonstrated.

To study whether persistent functional changes occur in intestinal ILC3s after microbial encounter, we used *Citrobacter rodentium*, a mouse pathogen that provokes an enterocolitis with disease similarities to human enteropathogenic *Escherichia coli* infection (13). *C. rodentium* attaches and effaces the distal small intestine and colon, provoking innate dendritic cell (DC)–induced ILC3 activation as well as generation of adaptive antigen-specific B and T cells (6, 9, 14). To focus on intestinal ILC3 responses to *C. rodentium* that are independent of adaptive immune priming (14) and infection-associated dysbiosis (13, 15), we limited the infection window using antibiotics (Abx) (15) (fig. S1, A to E). Indeed, a short course of ciprofloxacin was sufficient to restrict adaptive T helper type 22 (T_H22) responses, whereas innate ILC3-dependent IL-22 responses were activated normally (fig. S1, F to H). Although Abx treatment alone transiently modified intestinal bacterial communities (fig. S2, A to C), no long-term impact on ILC3 function (fig. S2, D to F) or on microbial diversity (fig. S3) was observed.

We characterized innate ILC3 and adaptive T_H22 immune responses in this modified *C. rodentium* infection model using *Rorc*^{GFP} and *Il22*^{TdT} reporter mice (16, 17) (Fig. 1, A and B; and fig. S4) (^{GFP}, green fluorescent protein; ^{TdT}, ^{TdT}omato). T cell and ILC3 populations were generally stable during the initial infection, but *C. rodentium* reinfection 1 month after Abx treatment resulted in a rapid increase in intestinal NKp46$^+$ and CCR6$^+$ ILC3 subsets with little effect on T cells (Fig. 1, B and C). Absolute numbers and frequencies of IL-22–expressing ILC3s increased in a similar fashion, whereas IL-22–expressing T cells were largely unchanged (Fig. 1, D to F; and fig. S5). *C. rodentium* challenge and rechallenge experiments in mice not treated with ciprofloxacin showed similar ILC3 responses, indicating the innocuous effects of the Abx treatment (fig. S6, A to C). CD4$^+$ T cell numbers and frequencies of IL-17A−, IL-22−, and interferon-γ (IFN-γ)–producing T cells were not affected (fig. S6, B to E). Thus, the homeostasis and function of intestinal IL-22–producing ILC3s can be selectively modified after an Abx-controlled subclinical *C. rodentium* infection.

Mucosal IL-22 production activates epithelial responses during pathogen infection and is required for resistance to *C. rodentium* (18, 19). Bacterial growth after first infection (denoted “CR”) was not observed after reinfection of Abx-cleared infected mice (denoted CR-AbxCR or “CRACR”) (Fig. 1, G and H), suggesting that enhanced ILC3 function in CRACR mice might play a role in the resistance to bacterial rechallenge. DC activation was noted during rechallenge, whereas monocytes, macrophages, and granulocytes were largely unchanged (fig. S7). Taken together, a limited initial exposure of intestinal ILC3s to pathogenic bacteria can generate a highly functional and persistent ILC3 subset, which we refer to hereafter as “trained ILC3s” (Tr-ILC3s).

Enhanced Tr-ILC3 responses persisted 4 months after *C. rodentium* reinfection of Abx-cleared mice (Fig. 2A), with reduced bacterial loads upon reinfection (Fig. 2B). Absolute numbers of total ILC3s (Fig. 2C) and IL-22$^+$ ILC3s (Fig. 2, D and E) were significantly increased in CRACR mice that were reinfected 4 months later with diverse ILC3 subsets as dominant IL-22 producers (Fig. 2, F and G). Because the DNA-binding protein inhibitor ID2 is highly expressed in differentiated ILCs (20, 21), we used *Id2*-regulated inducible fate-mapping (22) to track ILCs under steady state and after infection (Fig. 2H). All ILCs were red fluorescent protein (RFP)–labeled, with a somewhat higher percentage of RFP$^+$ ILC3s after *C. rodentium* infection (CR and CRA conditions; Fig. 2I). By contrast, most RFP$^+$ ILC1s and ILC2s were lost in CRACR mice, whereas labeled RFP$^+$ ILC3 subsets were maintained (Fig. 2I). These results indicate that diverse Tr-ILC3s can persist after a limited exposure to *C. rodentium* and may preferentially expand after pathogen reencounter.

We determined if Tr-ILC3s could be generated in the absence of adaptive immunity (Fig. 3A). Absolute numbers of IL-22$^+$ ILC3s were significantly increased in CRACR *Rag2*$^{-/-}$ mice (Fig. 3B), which had reduced bacterial loads compared with the CR-infected *Rag2*$^{-/-}$ mice (Fig. 3C). IL-22 production was required for Tr-ILC3–mediated protection against *C. rodentium* (Fig. 3A) because *Rag2*$^{-/-}$ *Il22*$^{-/-}$ CRACR mice did not survive reinfection (Fig. 3, D and E). We next compared the protective capacity of adoptively transferred naïve versus Tr-ILC3s in vivo (Fig. 3F). CR-infected *Il22*$^{-/-}$ mice that received naïve ILC3s exhibited body weight loss and succumbed about 2 weeks after infection (Fig. 3G). By contrast, CR-infected *Il22*$^{-/-}$ mice that received Tr-ILC3s recovered and survived (Fig. 3G). Thus, the enhanced functional capacity of Tr-ILC3s can be adoptively transferred and can operate in a T cell–independent fashion during pathogen rechallenge.

Although antigen specificity has long been considered as a cardinal feature of adaptive B and T cell memory (23), innate populations such as myeloid cells (24), natural killer (NK) cells (25, 26), and ILC2s (27) have been shown to have “memory-like” properties. To investigate pathogen-specific properties of Tr-ILC3s, we analyzed whether *C. rodentium*–activated Tr-ILC3s could protect against *Listeria monocytogenes. L. monocytogenes* infection (LM) elicits IL-23 release that can trigger ILC3 activation and IL-22 production, which is involved in the intestinal epithelial response (28). We found enhanced ILC3 responses after rechallenge with *L. monocytogenes* (CRALM compared with LM) (fig. S9, A and B). Thus, Tr-ILC3 responses are not restricted to *C. rodentium* and can potentially extend protection to unrelated pathogens. We also assessed whether Tr-ILC3s can be generated by cytokines alone. Although repeated IL-23 and IL-1β injection triggered higher IL-22 production in intestinal ILC3s (fig. S9, C and D), we failed to detect increased ILC3 numbers in this noninfectious context (fig. S9E). Tr-ILC3s therefore lack antigen specificity and require tissue-dependent signals beyond IL-1β and IL-23 for their generation.

RNA sequencing (RNA-seq) analysis on intestinal ILC3 subsets from naïve (C), *C. rodentium*–infected (CR), *C. rodentium*–infected and ciprofloxacin-treated (CRA), and CRACR mice allowed us to validate previous ILC3 datasets (5) and to identify more than 1000 genes in CCR6$^+$ ILC3s and 500 genes in CD49a$^+$ ILC3s modified by *C. rodentium* infection (Fig. 4, A and B; fig. S10A; and table S1). By contrast, comparison of CR and CRACR ILC3 profiles revealed only 152 differentially expressed genes in CCR6$^+$ ILC3s and

138 genes in CD49a$^+$ ILC3s, suggesting that altered transcriptomic profiles stably persist in ILC3s after *C. rodentium* infection (fig. S10, A and B). We documented increased effector functions in ILC3 subsets in *C. rodentium*–exposed mice compared with control naïve mice (Fig. 4C), with Tr-ILC3s strongly expressing transcripts for *Il22*, *Il17f*, *Gzmb*, and *Gzmc* (fig. S10C).

Classical and innate immunological memory requires metabolic rewiring (29, 30) that orchestrates cell survival, proliferation, differentiation, and long-term persistence of these cells. ILC3 subsets demonstrated a profound metabolic shift from glycolysis and glutaminolysis to enhanced tricarboxylic acid (TCA) cycle, oxidative phosphorylation (OXPHOS), fatty acid synthesis, and oxidation-associated gene expression after *C. rodentium* infection, which was preserved in CRA and CRACR mice (Fig. 4, C and D; and fig. S10C). As such, intestinal ILC3s experience durable metabolic rewiring after pathogen encounter.

Bioenergetic profiles, including extracellular acidification rate (ECAR) and cellular oxygen-consumption rate (OCR), define mitochondrial respiration and aerobic glycolytic activity, respectively. Tr-ILC3s showed higher OCRs, indicating increased mitochondrial fitness compared with naïve ILC3s (Fig. 4, E and F), although both required OXPHOS for IL-22 production (Fig. 4G). Diverse nutrients (including glucose, glumatine, and fatty acids) fuel immune cell metabolism and mitochondrial bioenergetic pathways (31). In addition, urea cycle–associated genes [arginase-1 (*Arg1*)] can drive ILC2 and T cell proliferation as well as proinflammatory functions (32, 33). Inhibition of glycolysis [2-deoxy-$_D$-glucose (2-DG)], glutamine conversion [bis-2-(5-phenylacetamido-1,3,4--thiadiazol-2-yl)ethyl sulfide (BPTES)], arginine metabolism [N^ω-hydroxy-nor-$_L$-arginine (Nor-NOHA)], or fatty acid β-oxidation (etomoxir) did not differentially affect IL-22 production from naïve versus Tr-ILC3s (fig. S10, D to F). However, combined treatment with 2-DG–BPTES and etomoxir significantly decreased IL-22 production from Tr-ILC3s, whereas Arg1 inhibition synergized with 2-DG, BPTES, and etomoxir to significantly reduce IL-22 production from naïve ILC3s (Fig. 4H). Therefore, $_L$-arginine may act as a metabolic source for naïve ILC3s but not Tr-ILC3s.

We further focused our attention on transcripts that were selectively modified in CRACR ILC3s (table S1). From the 51 transcripts that were up-regulated in both CD49$^+$ and CCR6$^+$ ILC3s, 12 were associated with the regulation of cell proliferation (Fig. 4I). Higher Ki67 levels were detected in ILC3s from CRACR compared with CR mice (Fig. 4J), consistent with rapid Tr-ILC3 proliferation after activation. Our results suggest that pathogen encounter is accompanied by durable metabolic changes in intestinal ILC3s, generating TrILC3 subsets with enhanced proliferative capacity and contributing to long-term mucosal defense.

Adaptive immune responses are classically associated with the development of immunological memory. The innate immune system can likewise adapt to environmental inflammatory signals that generate NK and myeloid cells with new long-lived phenotypes (24, 26). Here, we describe intestinal “trained” ILC3s that emerge and persist after initial pathogen encounter. Upon reinfection, Tr-ILC3s proliferate and robustly produce IL-22, thus promoting mucosal defense. The distinct metabolic activity in memory T cells (34, 35) and

trained monocytes and macrophages (24) is associated with epigenetic reprogramming. The precise mechanisms that underlie the distinct functional features of Tr-ILC3s and the signals that promote them remain to be defined. Tr-ILC3 targeting may provide an avenue for prevention or treatment of disease caused by inflammation or pathogens that invade barrier surfaces.

Supplementary Material

Refer to Web version on PubMed Central for supplementary material.

ACKNOWLEDGMENTS

We thank all the members of the Di Santo laboratory for critical review of the manuscript, helpful discussions, and support. We thank G. Eberl (Institut Pasteur, France) and O. Mandelboim (Hebrew University, Israel) for providing *Rorc*^{GFP} and *Ncr1*^{GFP} mice, respectively. We are indebted to S. Novault (Technology Core of the Center for Translational Science at Institut Pasteur, France) for cell sorting and M. Berard, R. Chennouf (Institut Pasteur, France, animal facilities), and M. Lecuit (Institut Pasteur, France) for support. We thank P. Bousso (Institut Pasteur, France) for critical comments on the manuscript.

Funding:

This work is supported by grants from the Institut National de la Santé et de la Recherche Médicale (INSERM), the Institut Pasteur, the Agence National pour le Recherche (ANR - ILC_MEMORY), and the European Research Council (ERC) under the European Union's Horizon 2020 research and innovation program (695467 – ILC_REACTIVITY). A.J. is supported by the French Ministry of Higher Education, Research, and Innovation and by the Fondation pour la recherche médicale.

Data and materials availability:

All data are available in the main text, supplementary materials, or public data repositories [16S rRNA at the NCBI Sequence Read Archive (SUB10763153/BioProject ID: PRJNA786093; RNA-seq datasets: GSE191167)].

REFERENCES AND NOTES

1. Hooper LV, Macpherson AJ, Nat. Rev. Immunol. 10, 159–169 (2010). [PubMed: 20182457]
2. Spits H et al., Nat. Rev. Immunol. 13, 145–149 (2013). [PubMed: 23348417]
3. Sonnenberg GF, Artis D, Nat. Med. 21, 698–708 (2015). [PubMed: 26121198]
4. Klose CSN, Artis D, Nat. Immunol. 17, 765–774 (2016). [PubMed: 27328006]
5. Robinette ML et al., Nat. Immunol. 16, 306–317 (2015). [PubMed: 25621825]
6. Satoh-Takayama N et al., Immunity 29, 958–970 (2008). [PubMed: 19084435]
7. Sonnenberg GF, Monticelli LA, Elloso MM, Fouser LA, Artis D, Immunity 34, 122–134 (2011). [PubMed: 21194981]
8. Buonocore S et al., Nature 464, 1371–1375 (2010). [PubMed: 20393462]
9. Cella M et al., Nature 457, 722–725 (2009). [PubMed: 18978771]
10. Yoshida H et al., Int. Immunol. 11, 643–655 (1999). [PubMed: 10330270]
11. Mebius RE, Rennert P, Weissman IL, Immunity 7, 493–504 (1997). [PubMed: 9354470]
12. Sawa S et al., Nat. Immunol. 12, 320–326 (2011). [PubMed: 21336274]
13. Collins JW et al., Nat. Rev. Microbiol. 12, 612–623 (2014). [PubMed: 25088150]
14. Basu R et al., Immunity 37, 1061–1075 (2012). [PubMed: 23200827]
15. Mullineaux-Sanders C et al., Cell Rep. 21, 3381–3389 (2017). [PubMed: 29262319]
16. Eberl G et al., Nat. Immunol. 5, 64–73 (2004). [PubMed: 14691482]

17. Shen W, Hixon JA, McLean MH, Li WQ, Durum SK, Front. Immunol. 6, 662 (2016). [PubMed: 26834739]
18. Wolk K et al., Immunity 21, 241–254 (2004). [PubMed: 15308104]
19. Zheng Y et al., Nat. Med. 14, 282–289 (2008). [PubMed: 18264109]
20. Cherrier M, Sawa S, Eberl G, J. Exp. Med. 209, 729–740 (2012). [PubMed: 22430492]
21. Xu W et al., Immunity 50, 1054–1068.e3 (2019). [PubMed: 30926235]
22. Rawlins EL, Clark CP, Xue Y, Hogan BL, Development 136, 3741–3745 (2009). [PubMed: 19855016]
23. Ordovas-Montanes J, Beyaz S, Rakoff-Nahoum S, Shalek AK, Nat. Rev. Immunol. 20, 308–320 (2020). [PubMed: 32015472]
24. Saeed S et al., Science 345, 1251086 (2014). [PubMed: 25258085]
25. Cooper MA et al., Proc. Natl. Acad. Sci. U.S.A. 106, 1915–1919 (2009). [PubMed: 19181844]
26. Sun JC, Beilke JN, Lanier LL, Nature 457, 557–561 (2009). [PubMed: 19136945]
27. Martinez-Gonzalez I et al., Immunity 45, 198–208 (2016). [PubMed: 27421705]
28. Disson O et al., J. Exp. Med. 215, 2936–2954 (2018). [PubMed: 30355616]
29. Arts RJW, Joosten LAB, Netea MG, Semin. Immunol. 28, 425–430 (2016). [PubMed: 27686054]
30. Bantug GR, Galluzzi L, Kroemer G, Hess C, Nat. Rev. Immunol. 18, 19–34 (2018). [PubMed: 28944771]
31. Muri J, Kopf M, Nat. Rev. Immunol. 21, 363–381 (2021). [PubMed: 33340021]
32. Geiger R et al., Cell 167, 829–842.e13 (2016). [PubMed: 27745970]
33. Monticelli LA et al., Nat. Immunol. 17, 656–665 (2016). [PubMed: 27043409]
34. Caputa G, Castoldi A, Pearce EJ, Nat. Immunol. 20, 793–801 (2019). [PubMed: 31213715]
35. Buck MD, O'Sullivan D, Pearce EL, J. Exp. Med. 212, 1345–1360 (2015). [PubMed: 26261266]

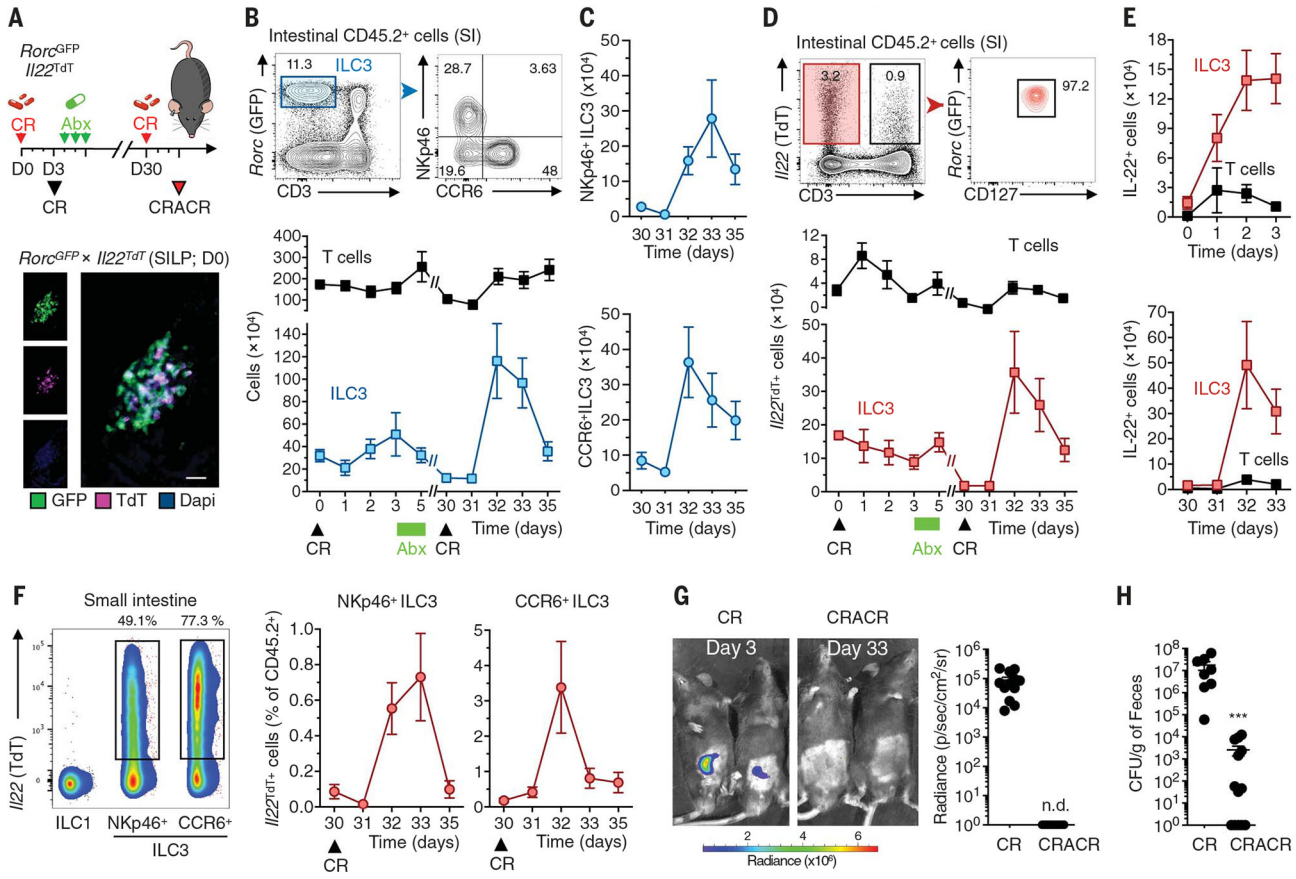

Fig. 1. Tr-ILC3s efficiently control pathogenic bacteria rechallenge.

(**A**) The experimental design for (B) to (H) is shown at the top. *Rorc*^{GFP}*Il22*^{TdT} mice received ciprofloxacin (Abx; 100 mg kg^{-1} day^{-1}) after *C. rodentium* infection (CR). One month later, the mice were reinfected with *C. rodentium* (CRACR). A representative steady-state immunofluorescence analysis of RORγt^{+} (green) and *Il22*$^{TdT+}$ (magenta) cells in the small intestine is shown at the bottom. Nuclei were stained with 4′,6-diamidino-2-phenylindole (DAPI) (blue) (scale bar, 20 μm). SILP, small intestine lamina propria; D0, day 0. (**B**) Intestinal NKp46^{+} and CCR6^{+} ILC3s were analyzed by flow cytometry (top). Absolute numbers of ILC3s and T cells in the small intestine lamina propria (*n* = 4 to 12 for each time point) are shown at the bottom. (**C**) Absolute numbers of intestinal NKp46^{+} (top) and CCR6^{+} (bottom) ILC3s determined with representative data from three independent analyses (*n* = 3 to 7 for each time point). (**D**) Small intestinal *Il22*$^{TdT+}$ ILC3 (CD45^{+}CD3^{-}*Rorc*$^{GFP+}$) and T cell (CD45^{+}CD3^{+}) frequencies at day 0 (top). Absolute numbers of *Il22*$^{TdT+}$ cells were determined with representative data from six independent analyses (*n* = 4 to 12 for each time point) (bottom). (**E**) Absolute numbers of IL-22^{+} (protein) cells were analyzed after ex vivo IL-23 (top) and IL-1β (bottom) stimulation (*n* = 4 to 9 for each time point). (**F**) *Il22*^{TdT} expression in ILC1s (CD3^{-}NKp46^{+}NK1.1^{+}), NKp46^{+} ILC3s, and CCR6^{+} ILC3s (left). Representative data are from three independent analyses. The frequencies of *Il22*$^{TdT+}$NKp46^{+} and NKp46^{-} ILC3 subsets in the small intestine lamina propria after reinfection are shown on the right (CRACR; *n* = 3 to 7 for each time point). (**G**) *C. rodentium* growth monitored by IVIS imaging (CR, *n* = 12; CRACR, *n*

= 12). Representative pseudocolor images are shown (color scale in photons s^{-1} cm^{-2} sr^{-1}). (**H**) Fecal *C. rodentium* counts (CR, $n = 8$; CRACR, $n = 13$). Data are representative of three independent experiments. Each graph corresponds to the mean ± SEM of the values obtained. n.d. indicates not detected and ***$P < 0.001$ using two-tailed Mann-Whitney test.

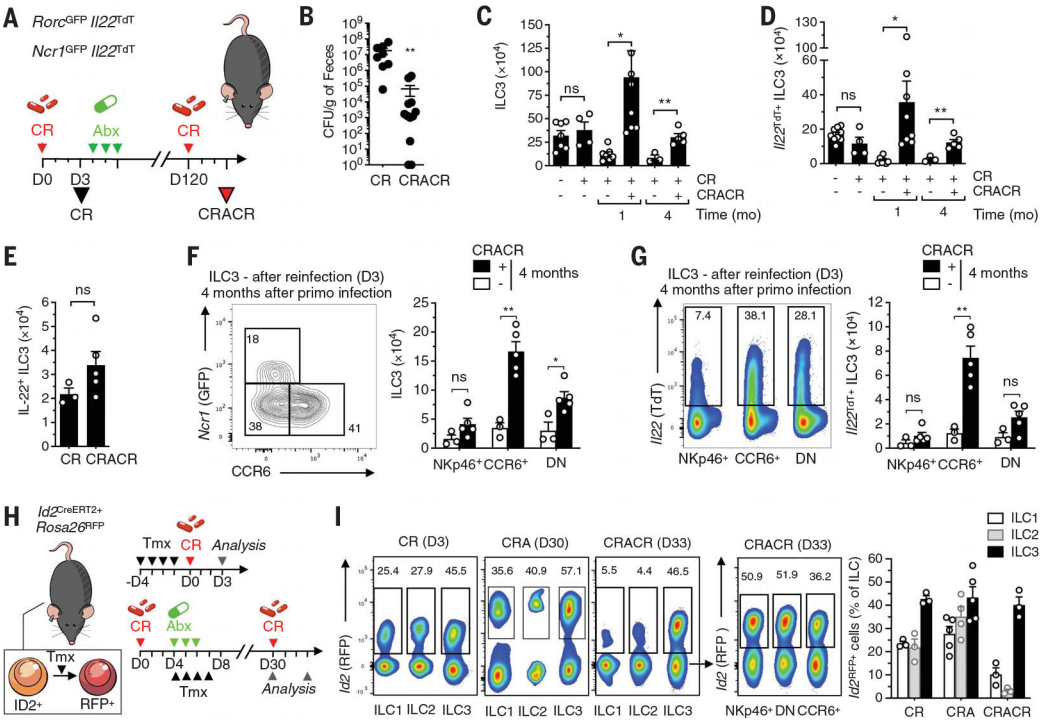

Fig. 2. Tr-ILC3s show long-term persistence.

(**A**) Experimental design for (B) to (H). *Rorc*^{GFP}×*Il22*^{TdT} and *Ncr1*^{GFP}×*Il22*^{TdT} mice received ciprofloxacin (Abx; 100 mg kg^{-1} day^{-1}) after *C. rodentium* infection. Four months later, the mice were reinfected with *C. rodentium* (CRACR). (**B**) Fecal *C. rodentium* counts (CR, $n = 8$; CRACR, $n = 12$). CFU, colony forming units. (**C** and **D**) Absolute numbers of total (C) ($n = 3$ to 8) and *Il22*^{TdT}+ (D) ($n = 3$ to 9) ILC3s in the small intestine lamina propria. (**E**) Absolute numbers of intestinal IL-22+ ILC3s (protein; $n = 3$ to 5) after ex vivo IL-23 and IL-1β stimulation 3 days after infection or reinfection. (**F** and **G**) Frequency and absolute numbers of ILC3s (F) and *Il22*^{TdT}+ ILC3 (G) subsets in CRACR mice were determined ($n = 3$ to 5). DN, double negative. (**H**) Fate-mapping protocol. *Id2*$^{CreERT2+}$×*Rosa26*^{RFP} mice received ciprofloxacin (Abx; 100 mg kg^{-1} day^{-1}) 3 days after *C. rodentium* infection. Mice received tamoxifen (Tmx) by intraperitoneal injection and were analyzed as shown. (**I**) Analysis of *Id2*$^{RFP+}$ cells in ILC1 (CD3^{-} NKp46^{+}NK1.1^{+}), ILC2 (CD3^{-}CD127+ CD90.2^{+}KLRG1^{+}), and ILC3 subsets (left) for the protocol shown in (H). Percentages of *Id2*$^{RFP+}$ cells of the total ILCs in CR, CRA, and CRACR mice were determined ($n = 3$ to 5) (right). Each graph corresponds to the mean ± SEM of the values obtained. ns indicates not significant, $*P < 0.05$, and $**P < 0.01$ using two-tailed Mann-Whitney test.

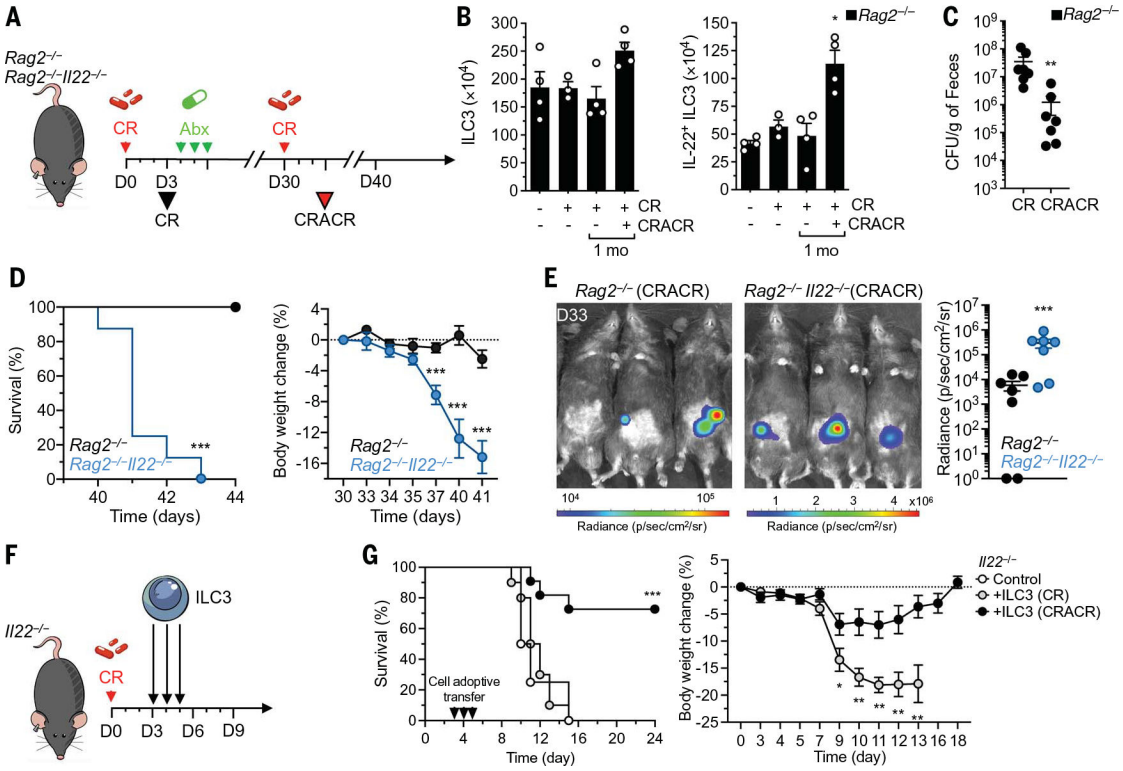

Fig. 3. Tr-ILC3s show enhanced IL-22–mediated protection.

(**A**) Experimental design for (B) to (E). *Rag2*$^{-/-}$ and *Rag2*$^{-/-}$ *Il22*$^{-/-}$ mice received ciprofloxacin (Abx; 100 mg kg^{-1} day^{-1}) after *C. rodentium* infection. One month later, the mice were reinfected with CR (CRACR). (**B**) Analysis of ILC3s (left) and IL-22^{+} ILC3s (right) in *Rag2*$^{-/-}$ mice (n = 3 to 4). (**C**) Fecal *C. rodentium* counts (n = 7). (**D**) Survival (left) and body weight (right) in reinfected *Rag2*$^{-/-}$ and *Rag2*$^{-/-}$ *IL22*$^{-/-}$ mice (n = 7). (**E**) *C. rodentium* growth monitored by IVIS imaging 3 days after reinfection (left). Relative *C. rodentium* growth was determined in *Rag2*$^{-/-}$ and *Rag2*$^{-/-}$ *IL22*$^{-/-}$ mice (n = 7) (right). (**F**) Experimental design for (G). ILC3s were purified from infected (CR) or reinfected (CRACR) mice 3 days after infection and transferred into *C. rodentium*–infected *Il22*$^{-/-}$ mice. (G) Survival and body weight were assessed at the indicated times after infection [n = 4 for *Il22*$^{-/-}$ and ILC3 (CR); n = 10 for *Il22*$^{-/-}$ and ILC3 (CRACR); n = 11 for *Il22*$^{-/-}$ per group, pool of two independent experiments]. Each graph corresponds to the mean ± SEM of the values obtained. *P < 0.05, **P < 0.01, and ***P < 0.001 using Krustal-Wallis test (B), two-tailed Mann-Whitney test [(C) to (G)], or log-rank (Mantel-Cox) test [(D) and (G)].

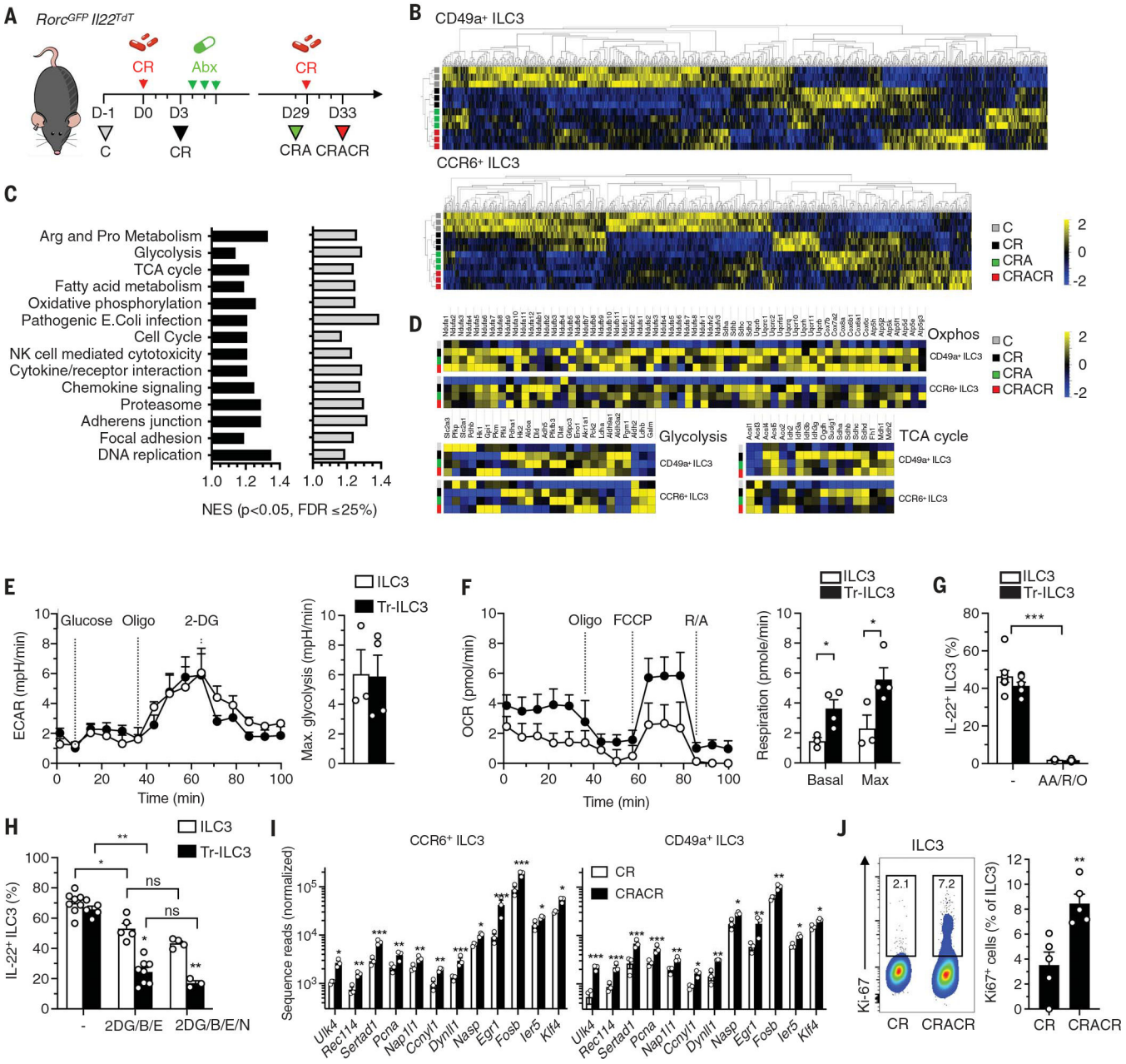

Fig. 4. Gene expression analysis and metabolic profiles of Tr-ILC3s.

(*A*) CCR6$^+$ and CD49a$^+$ ILC3 from naïve (C) and infected mice (CR, CRA, and CRACR) were sorted for RNA-seq analysis. (**B** and **C**) A heatmap showing the relative expression levels of differentially expressed genes is shown in (B). In (C), pathway analysis was performed and gene pathways were organized into clusters to compare CR, CRA, and CRACR conditions to C ($n = 3$). FDR, false discovery rate; NES, normalized enrichment score. (**D**) Heatmap with clustering of differentially expressed metabolism-associated genes ($n = 3$). (**E** and **F**) Seahorse analysis of freshly sorted ILC3s (C) and Tr-ILC3s (CRACR) in response to a mitochondrial uncoupler [fluoro-carbonylcyanide phenylhydrazone (FCCP)], oligomycin (oligo), rotenone and antimycin (R/A), and 2-DG. Representative metabolic

profiles (OCR and ECAR), glycolysis, and respiration were determined (three independent experiments; $n = 3$ to 4). (**G**) Effect of OXPHOS inhibition (18 hours) on IL-22 production by intestinal ILC3s ($n = 5$). AA, antimycin; R, rotenone; O, oligomycin. (**H**) Effect of metabolic pathway inhibition (2 hours) on IL-22 production by intestinal ILC3s (two independent experiments; $n = 3$ to 8). B, BPTES; E, etomoxir; N, Nor-NOHA. (**I**) Differentially expressed genes in CR and CRACR ILC3s ($n = 3$). (**J**) Frequency of $Ki67^+$ ILC3 from infected (CR) and reinfected (CRACR) mice (two independent experiments; $n = 5$). Each graph corresponds to the mean ± SEM of the values obtained. ns indicates not significant, $*P < 0.05$, $**P < 0.01$, and $***P < 0.001$ using two-tailed unpaired Student's t test [(E) and (F)], two-tailed Mann-Whitney test [(G) and (J)], or Krustal-Wallis test (H).